Journal of Electroceramics, 8, 37–48, 2002

Microstructural, Dielectric, Pyroelectric and Ferroelectric Studies on Partially Grain-Oriented $SrBi_2Ta_2O_9$ Ceramics

G. SENTHIL MURUGAN & K.B.R. VARMA*
Materials Research Centre, Indian Institute of Science, Bangalore 560012, India
kbrvarma@mrc.iisc.ernet.in

Submitted July 9, 2001; Revised December 12, 2001; Accepted January 24, 2002

Abstract. Partially grain-oriented (48%) ceramics of strontium bismuth tantalate ($SrBi_2Ta_2O_9$) have been fabricated via conventional sintering. The grain-orientation factor of the ceramics was determined, as a function of both the sintering temperature and duration of sintering using X-ray powder diffraction (XRD) techniques. Variations in microstructural features (from acircular to plate like morphology) as a function of sintering temperature of the pellets were monitored by Scanning Electron Microscopy (SEM). The dielectric constant and loss measurements as functions of both frequency and temperature have been carried out along the directions parallel and perpendicular to the pressing axis. The anisotropy ($\varepsilon_{rn}/\varepsilon_{rp}$) associated was found to be 2.21. The effective dielectric constant of the samples with varying porosity was predicted using different dielectric mixture formulae. The grain boundary and grain interior contributions to the dielectric properties were rationalized using the impedance spectroscopy. The pyroelectric coefficient for strontium bismuth tantalate ceramic was determined along the parallel and perpendicular directions to the pressing axis and found to be -23 $\mu C/m^2K$ and -71 $\mu C/m^2K$, respectively at 300 K. The ferroelectric properties of these partially grain-oriented ceramics are superior in the direction perpendicular to the pressing axis to that in the parallel direction.

Keywords: electroceramics, grain-orientation, strontium bismuth tantalate, scanning electron microscopy, dielectric, hysteresis loop

1. Introduction

In recent years, there has been a tremendous interest in the ferroelectric thin films in view of their potential applications in electronic devices such as electro-optic modulators, pyroelectric infrared detectors, optical switches, microelectronic mechanical systems and non-volatile random access memory (NVRAM) [1–4]. One of the candidate materials chosen for these applications and most widely studied is $PbZr_{(1-x)}Ti_xO_3$ (PZT) because of its highest switching polarization combined with low switching field. However, apart from Pb toxicity, PZT (in particular with metallic electrodes) suffers from serious degrading problems such as fatigue (a decrease in the amount of switchable polarization in each time after about 10^8 read/write cycles), ageing and leakage current that hinder the usability of this material in devices [5–9]. During the search for an alternate ferroelectric material for these applications, it was found that bismuth oxide layered structures (e.g., $SrBi_2Ta_2O_9$, $BaBi_2Ta_2O_9$, $SrBi_2Nb_2O_9$) originally synthesized by Aurivillius [10] are the most suitable ones. The general formula for Aurivillius family of layered oxides is $[Bi_2O_2]^{2+}$ $[A_{n-1}B_nO_{3n+1}]^{2-}$, where A is a combination of cations adequate for 12-coordination such as K^+, Na^+, Ca^{2+}, Sr^{2+}, Pb^{2+}, Ba^{2+}, Ln^{3+} etc., B is a combination of cations suitable for octahedral coordination like Fe^{3+}, Ti^{4+}, Nb^{5+}, Ta^{5+}, W^{6+} etc. and n is an integer, varies from 1–5, and corresponds to the number of perovskite like structures stacked in between Bi_2O_2 layers. $SrBi_2Ta_2O_9$ (SBT), which is an $n=2$ member of the above family of layered compounds, proved to be the versatile material for multifarious applications. It contains two perovskite-like

*To whom all correspondence should be addressed.

TaO_6 octahedron units stacked in between $[Bi_2O_2]^{2+}$ layers along *c*-axis and strontium cations are located in the space between TaO_6 octahedrons. The lattice of SBT, consisting of perovskite (TaO_6) octahedra separated by $[Bi_2O_2]^{2+}$ planes give rise to spontaneous polarization along the planes (i.e. *a* or *b* axis) [11, 12]. The crystal structure has orthorhombic symmetry with $a = 5.5306$, $b = 5.5344$ and $c = 24.9839$ Å. SBT films exhibit large polarization associated with small coercive field with no ferroelectric fatigue even after 10^{12} cycles of switching. Also it has good retention properties and low leakage current on platinum electrodes [13–17].

The fatigue free nature of SBT films was explained using many theories and models [18]. There exists vast literature on SBT thin films for a variety of applications with major emphasis on NVRAM devices. Though there exists an abundant literature on the science and technology of thin films of SBT, to the best of the knowledge of the authors the data available on polycrystalline SBT is scanty [18, 19] and has yet to be fully explored in bulk form for various properties and applications. It is known in the literature that the piezoelectric properties of conventionally sintered ceramics of the above family of bismuth based compounds with layered structure are not significantly large [20]. One of the reasons for this particular behavior is understood to be the restriction of the permissible rotations of the spontaneous polarization in two dimensions (*a*-*b* plane) as compared to the freedom along all three dimensions in the ferroelectrics of the perovskite type compounds. Novel processing methods to fabricate grain-oriented ceramic were contemplated. Grain-oriented ceramics of $Bi_4Ti_3O_{12}$ and $PbBi_4Ti_4O_{15}$ obtained by hot forging techniques yielded improved dielectric and ferroelectric properties [21–23]. Molten salt synthesis followed by either tape casting or conventional sintering techniques yielded good grain-oriented ceramics of the Aurivillius family of ferroelectric oxides [24, 25]. Another fascinating route of preparing grain-oriented ceramics has been glass–ceramic by which one could also achieve strict control over the crystallite size and hence the physical properties [26–28]. It is with this interest that we have been making attempts to fabricate and characterize glass nanocomposites containing SBT nanocrystallites [29]. To begin with, we thought it is worth investigating into the influence of microstructural effects on the dielectric, pyroelectric and ferroelectric properties of the title compound in the bulk polycrystalline form. The present paper describes the details pertaining to these aspects of SBT ceramics.

2. Experimental

Polycrystalline ceramic powder of SBT was prepared by conventional solid state reaction route. Stoichiometric mixture of $SrCO_3$, Bi_2O_3 and Ta_2O_5 (Aldrich Chemicals) of 99.99% purity were heated at 1370 K for 12 h, in air with intermediate grinding and heating stages. The phase formation of the as-prepared powder was confirmed via X-ray powder diffraction (XRD) (Scintag Inc. USA) using Cu Kα radiation. The as-prepared powder was then cold pressed at 300 K for a few minutes at the pressure of 300 Kg/cm^2. Partially grain-oriented samples were obtained by subjecting these pressed pellets to the conventional sintering. The pellets were sintered at various temperatures for different durations. The samples sintered at 1370 K for 6 h will be referred to as 1370 K/6 h and those for 10 h as 1370 K/10 h and like wise for the other durations and temperatures in the forthcoming sections of the paper.

The sintered pellets were subjected to XRD studies for phase identification. The comparison of XRD patterns of the sintered pellets with that of the as-prepared polycrystalline powder over the 2θ range of 5° to 70° enabled to evaluate the degree of grain-orientation f. The degree of grain-orientation, f was calculated [30] using the formula

$$f = \frac{(P - P_0)}{(1 - P_0)}$$

where P is the ratio of the sum of intensities of the oriented peaks to the sum of intensities of all the peaks including oriented peaks for the grain-oriented pellet. P_0 is the similar ratio referring to the non-oriented polycrystalline powder.

The densities (ρ) of the sintered pellets were determined by Archimedian's principle using xylene (density = 0.86 g cm^{-3}) as the liquid medium. The porosity of the pellets were calculated using the relation $P = (\rho_T - \rho/\rho_T)$, where ρ_T is the theoretical density for SBT (8.785 g cm^{-3}) [31]. The microstructures of the sintered pellets were studied using Scanning Electron Microscopy (SEM) (Leica 440I, Oxford Instruments). The grain size was calculated from the scanning electron micrograph using the image analysis software (Quantimet MC 500) associated with SEM.

The capacitance and dielectric loss measurements were carried out on the polished pellets with gold electrodes sputtered on the surface. Copper leads were attached to the gold electrodes using silver epoxy. These measurements were made as functions of both frequency (100 Hz–1 MHz) and temperature (300 K–670 K), using an impedance gain phase analyser (HP 4194A) at a signal strength of 0.5 V_{rms}.

The ferroelectric hysteresis loop (P vs E) was recorded at a switching frequency 50 Hz with a modified Sawyer–Tower circuit [32]. The values of remnant polarization (P_r) and the coercive field (E_c) were determined from the hysteresis loop. The pyroelectric coefficient of the present ceramic was determined by Byer and Roundy method [33]. Prior to this measurement the samples were electrically poled with a dc field of 5–6 kV/cm at 520 K and subsequently these were short-circuited to eliminate the surface charges. The sample was placed in a programmable furnace, heated at a uniform rate and the pyroelectric current developed was monitored using a Keithley 485 autoranging picoammeter. The pyroelectric current (I) produced parallel to the poling axis due to the variation of the spontaneous polarization (P_s), with temperature is given by

$$I = A \times p(T) \frac{dT}{dt}$$

where $p(T) = dP_s(T)/dT$ is the pyroelectric coefficient calculated at a temperature T, A is the electrode area normal to the polar (i.e. poling) axis and dT/dt is the heating rate.

3. Results and Discussion

3.1. *Structural Studies and Degree of Grain-Orientation*

The XRD patterns recorded for the faces perpendicular to the pressing axis of the 1370 K/10 h, 1420 K/10 h, 1470 K/10 h and 1520 K/10 h samples (pellets) are shown in the Fig. 1(a)–(d). For comparison, the XRD pattern for the randomly oriented as-prepared polycrystalline powder is also included in Fig. 1(e). These studies confirm the absence of oriented grain growth in the direction perpendicular to the (00ℓ) plane. However, we find preferential orientation in the $[11\ell]$ direction (peaks with arrow marks in Fig. 1). Interestingly, the growth of grains seems to take place only in the direction of c-axis keeping the intercept with the ab plane constant. Similar trend has been reported in grain-oriented lanthanum borogermanate glass-ceramic [34]. The dielectric studies carried out in the direction parallel to the cold pressing axis show lower dielectric constant (discussed in the forthcoming section) indicating that the axis parallel to the pressing direction is close to c axis, which is referred to as non-polar axis in these layered oxides [11, 12].

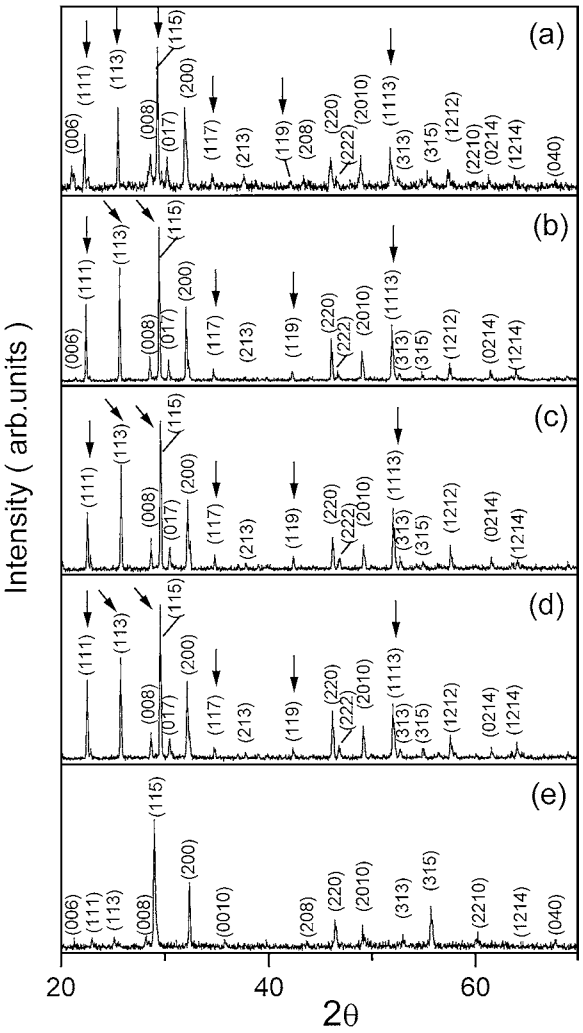

Fig. 1. The XRD patterns recorded for the faces perpendicular to the pressing axis for (a) 1370 K/10, (b) 1420 K/10 h, (c) 1470 K/10 h and (d) 1520 K/10 h samples and (e) for randomly oriented as-prepared polycrystalline powder.

The degree of grain-orientation (f) in these sintered pellets along the $[11\ell]$ direction is tabulated in the Table 1. Among the pellets sintered at four different temperatures for the same duration (10 h), the one

Table 1. The average dimensions of the grain calculated from the scanning electron micrograph and the grain-orientation factor found from XRD for the samples sintered at different temperatures for 10 h.

Sl. no	Sintering temperature (K)	Area (μm^2)	Length (μm)	Breadth (μm)	Aspect ratio	Orientation factor (f)
1	1370	18.25	8.76	3.33	2.73	0.34
2	1420	36.43	15.95	3.94	4.21	0.48
3	1470	55.17	21.19	3.96	5.51	0.42
4	1520	98.68	28.99	5.54	5.88	0.44

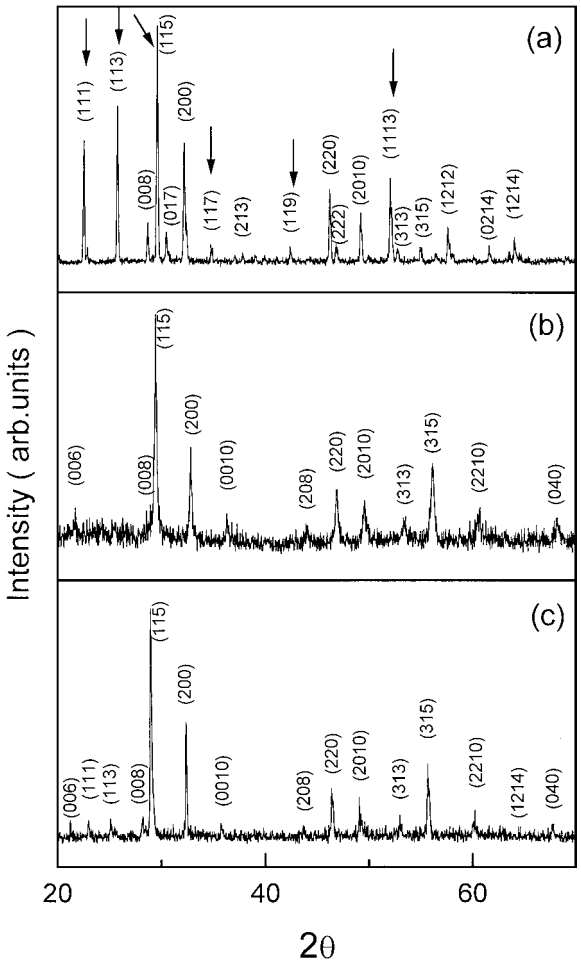

Fig. 2. The XRD patterns for (a) perpendicular and (b) parallel faces of grain-oriented 1520 K/10 h samples and (c) for randomly oriented as-prepared polycrystalline powder.

sintered at 1420 K shows large f (i.e., 0.48). Figure 2(a) and (b) depicts the XRD patterns recorded for the faces perpendicular and parallel to the pressing axis of the 1520 K/10 h sample respectively. For a quick reference, the XRD recorded for the polycrystalline ceramic powder is also included in Fig. 2(c). In Fig. 2(b), we clearly notice the absence of (111), (113), (117), (119) and (1113) peaks and a decrease in the intensity of (115). Indeed this observation unambiguously confirms the occurrence of partial grain-orientation in the face perpendicular to the pressing axis.

3.2. *Microstructural Analyses*

Scanning electron microscopic investigations were carried out systematically to unravel the underlying microstructural features of the surfaces perpendicular to the pressing axis of the 1370 K/10 h, 1420 K/10 h, 1470 K/10 h and 1520 K/10 h samples. Figure 3(a) and (b) shows the scanning electron micrographs obtained for the representative 1370 K and 1520 K heat treated samples. These micrographs demonstrate the presence of elongated grains that are aligned in the plane perpendicular to the pressing axis. However, the areas of the grains seem to be increasing with increase in sintering temperature. The results obtained in the XRD analyses are also inline with these studies. The orientation factor, f (Table 1) of the 1370 K/10 h sample is lower to a great extent than that of the other three samples (1420 K/10 h, 1470 K/10 h and 1520 K/10 h), as is evidenced in the micrograph (Fig. 3(a)). The average length, breadth, area and aspect ratio of the grains were calculated from the micrographs and found to increase with increase in sintering temperatures (Table 1). It was also noted that the 1470 K/10 h and 1520 K/10 h samples were more porous than the other two. Interestingly, the sample sintered at 1420 K/10 h gives rise to a dense microstructure than those of other three samples. Incidentally, the f of this sample is also higher than the other three samples under study, which may be attributed to the presence of less porous dense microstructure. High porosity in the ceramics will impede the grain-orientation by providing them with the required degree of freedom.

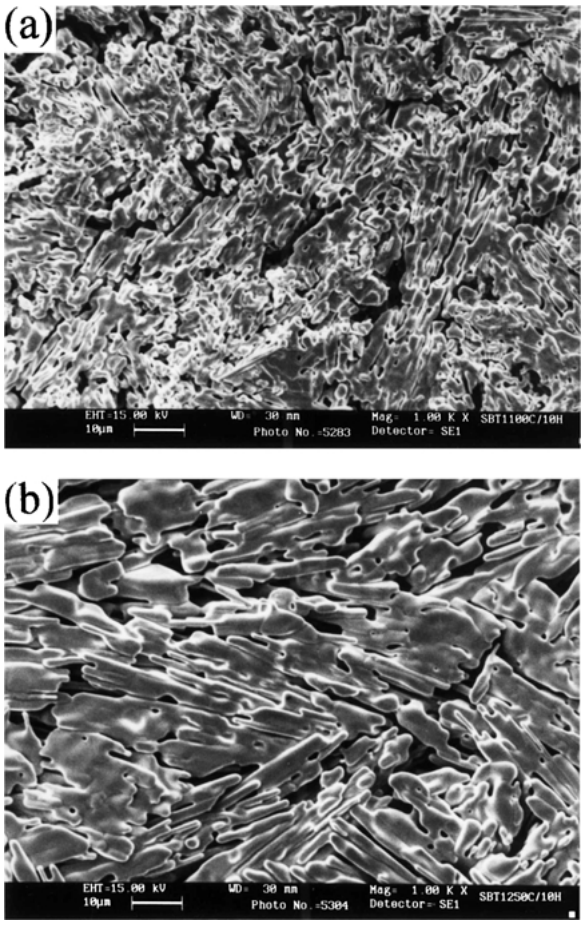

Fig. 3. The scanning electron micrographs for (a) 1370 K/10, and (b) 1520 K/10 h samples recorded on the surface perpendicular to the pressing axis.

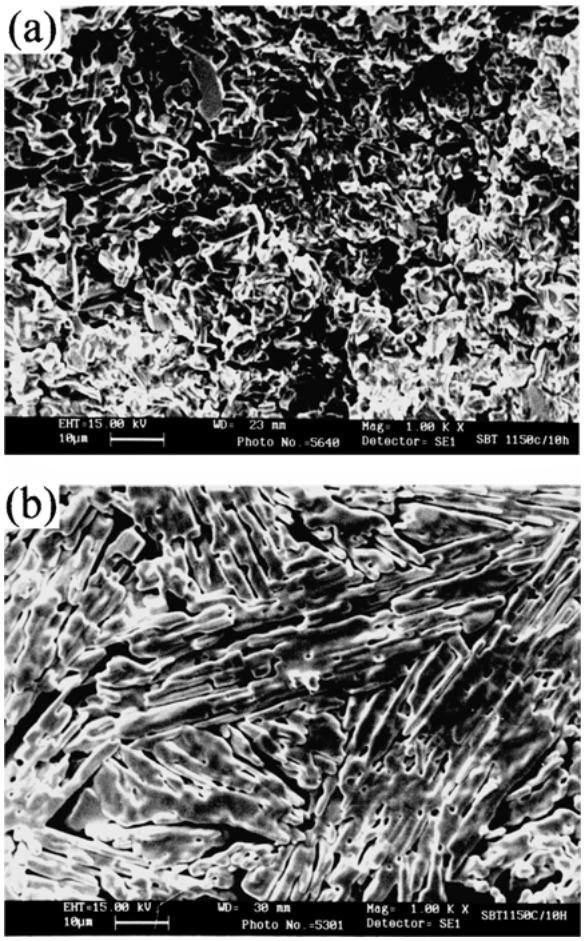

Fig. 4. The scanning electron micrographs recorded on the surfaces (a) parallel and (b) perpendicular to the pressing axis for 1420 K/10 h sample.

To visualize the influence of the duration of sintering on the microstructure and physical properties, the SBT ceramics were sintered at 1470 K for different durations (6, 10, 15 and 20 h). Though there is minor increase in the grain size, the duration of sintering does not seem to have any significant effect on the microstructure. However, the 20 h sintered pellet shows a fusion of adjacent grains and loses distinct morphology. Figure 4(a) and (b) shows the SEM for the 1420 K/10 h sample, recorded on the surfaces parallel and perpendicular to the pressing direction respectively. Figure 4(a) does not show any preferred orientation and the grains are randomly oriented. There is a clear indication of higher grain growth only in the direction normal to the pressing axis. These results were akin to those reported for the other layered bismuth compounds [22, 24, 35].

The experimental density and the percentage of porosity of the samples sintered at different temperatures for the same duration (10 h) is shown in Fig. 5. There is a small increase in the density from 1370 K to 1420 K. Further increase in the sintering temperature leads to a sudden decrease in the density due to the excessive directional grain growth which results in loose packing of the matrix as evidenced in SEM (Fig. 3). Apart from this, the loss of Bi_2O_3arising out of sintering the pellets at elevated temperatures could contribute to the observed decrease in density. Similar observations were made on the other materials of Aurivillius family of ferroelectric oxides [36, 24]. $BaBi_2Ta_2O_9$ ceramics sintered in the 1120 K–1170 K temperature range were found to have a microstructure containing rod like grains and the density increased

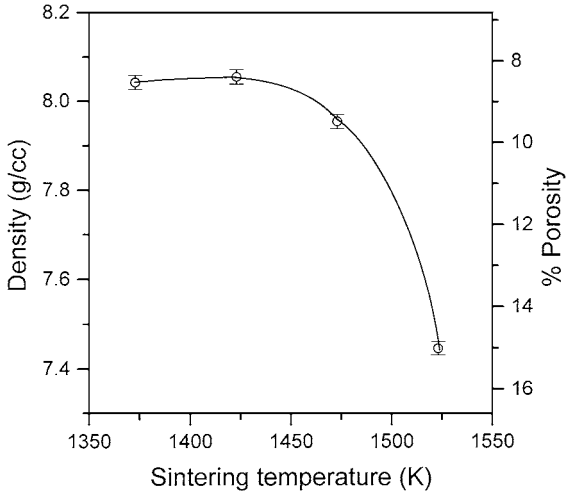

Fig. 5. Density and percentage porosity as a function of sintering temperature.

with increase in sintering temperature and suddenly decreased to a much lower value on further rise in sintering temperature [36].

3.3. Dielectric Studies

The dielectric constant (ε_r) and dielectric loss (D) as a function of frequency at room temperature, measured along the parallel (ε_{rp} and D_p) and the normal (ε_{rn} and D_n) directions to the pressing axis are shown in Fig. 6(a) and (b). The ε_r of the samples measured parallel to the direction of pressing axis (ε_{rp}) does not have any significant frequency dispersion i.e. not more than 1% through out the frequency range selected in the present study. Eventhough, there were reports on the influence of increase in grain size on ε_r of the present kind of ceramics [37, 38], no reference has been made to its porosity. We believe that the decrease in ε_r with an abnormal increase in grain size is chiefly due to the excessive porosity that is associated with these ceramics. In a situation of this kind, one may invoke the dielectric mixture formulae that are normally employed to predict the dielectric constants of two phase composite. In the present case, the crystallites of SBT and the porosity have been considered to form two phases of the models that we are going to tackle in the latter part of this section. The dielectric constant measured along the normal direction to the pressing axis (ε_{rn}) of the 1520 K/10 h sample showed enhanced dielectric constant (135) than that (61) measured in the other direction despite the

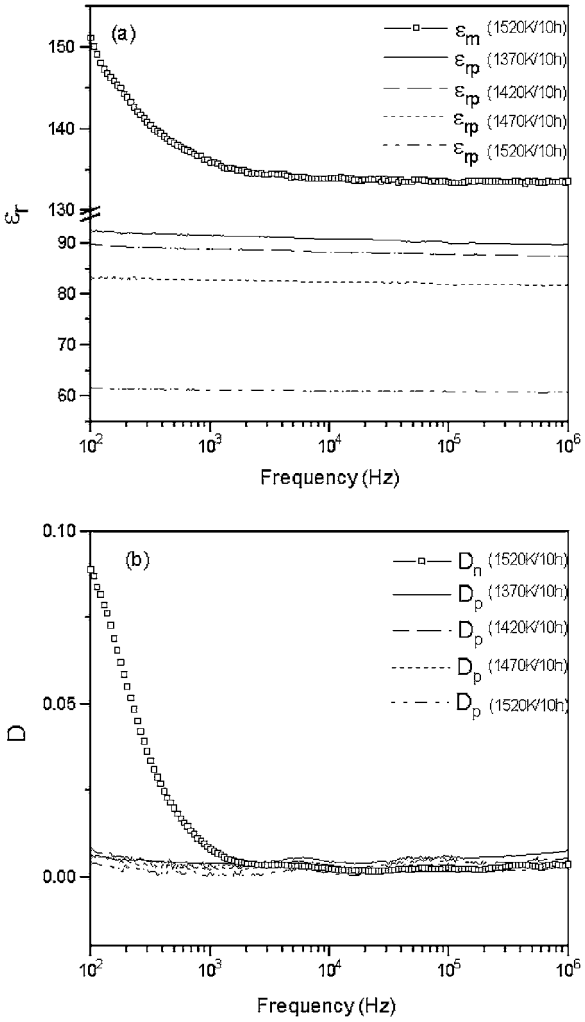

Fig. 6. The variation of (a) ε_{rn} and ε_{rp} and (b) D_n and D_p, with frequency at 300 K for different samples.

porous nature of the sample. In addition to the high dielectric constant, the dielectric dispersion in the low frequency range is also higher, which may be attributed to the interfacial polarization arising from grain boundary regions. The significant dielectric anisotropy that is observed in the present samples is rationalized in the following way.

Since the structure of SBT consists of perovskite layers parallel to the *a* and *b* axes, the polar axis lies in the *c*-plane. The dielectric constant along any axis in the *c*-plane is expected to be higher than the one measured normal to the *c*-plane. In the present case, since most grains are aligned with their *c*-axes along the pressing direction, the dielectric constant measured

perpendicular to the pressing axis (*a* or *b* axis) is higher. The value of ε_{rn} in the present case with $f = 0.44$ was 135 (at 100 kHz) while the ε_r value reported for hot forged SBT with $f = 0.52$ was 189 (at 100 kHz) and for the non-oriented conventionally fired dense ceramic it was 135 (at 100 kHz, 300 K) [39]. The lower value of the present ceramic is ascribed to the porous nature and low f of the sample. The dielectric loss of the different samples measured along the parallel direction to the pressing axis show almost same values of $D(\approx 0.01)$ (Fig. 6(b)). It is almost independent of both frequency and grain size in this direction, while the loss along the normal direction to the pressing axis also behaves in a similar manner except for the low frequency dispersion.

The ceramic under investigations are considered to be diphasic materials in which pores of volume fraction V_1 (having dielectric constant $\varepsilon_1 = 1$) are uniformly distributed in the matrix of SBT of volume fraction V_2 (dielectric constant ε_2). For polarisable spheres dispersed in continuous loss less medium, the Clausius-Mossotti relation [40] could be used to predict the effective dielectric constant (ε_{eff}). Since the present system does not satisfy this condition, the dielectric constant predicted based on Clausius-Mossotti relation is away from the experimental value . A commonly used dielectric mixture law is that of Litchtenecker [41], widely known as logarithmic mixture rule which is derived as an intermediate form of the series and parallel combination laws for dielectrics. The ε_{eff} values obtained using this rule are not in agreement with the experimental value because of a large difference in the ε_r values of the two phases. However, one of the generalized formulae proposed by Wiener [42, 43]

$$\frac{\varepsilon_{eff} - \varepsilon_2}{\varepsilon_{eff} + \varepsilon_2} = V_1 \frac{\varepsilon_1 - \varepsilon_2}{\varepsilon_1 + \varepsilon_2}$$

which takes into account the cylindrical shape of the phase 1 (pores) shows best fit for the experimental value obtained for all the samples under investigation. The effective dielectric constant (92) calculated using the above formula (at $V_1 = 0.0845$) is close to the experimentally observed dielectric constant (90, at 100 kHz, 300 K). The dielectric constant values that are obtained for different volume fractions of pores are in agreement with the experimental value. It is indeed consistent with the microstructural studies (Fig. 3).

Figure 7 shows the temperature dependence of ε_r measured for ceramics sintered at different temperatures along the direction parallel to the pressing axis. It

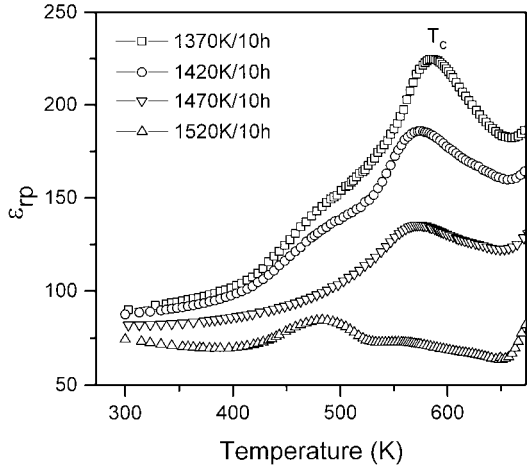

Fig. 7. The temperature dependence of ε_{rp} (at 100 kHz) for the samples sintered at different temperatures for 10 h.

is evident from this curve that there is a broad transition around 470 K which is in the same range as that reported using optical birefringence [44] measurements. It is known in the literature that even layered ($n = 2$) compounds of this family show two phase transitions. It is noticed that as the sintering temperature increases the ferroelectric to paraelectric transition temperature, T_c shifts towards lower temperature and the peak broadens. The dielectric studies on Barium Titanate and Barium Strontium Titanate [45, 46] also yielded similar results with increase in grain size. In the present material the T_c has a directional dependency. The ε_{rn} ($\perp$ direction) shows higher T_c than the one observed in ε_{rp} for all the samples. The typical variation of ε_r with temperature for the representative sample (1520 K/10 h) in both the directions is shown in Fig. 8. The ε_{rn} values are higher than ε_{rp} values both at 300 K and in the vicinity of T_c. The strong hump that we see around 470 K in the curve corresponding to ε_{rp} confirms the incidence of a phase transition. However, the absence of sharp distinct maximum on the ε_r vs T curve, expected in the vicinity of the ferroelectric to paraelectric transition, is attributed mainly to the presence of excessive porosity in these samples.

3.4. Impedance Analysis

Electrical transport properties of the polycrystalline ceramics are known to be strongly effected by their microstructures. Impedance spectra, which accurately

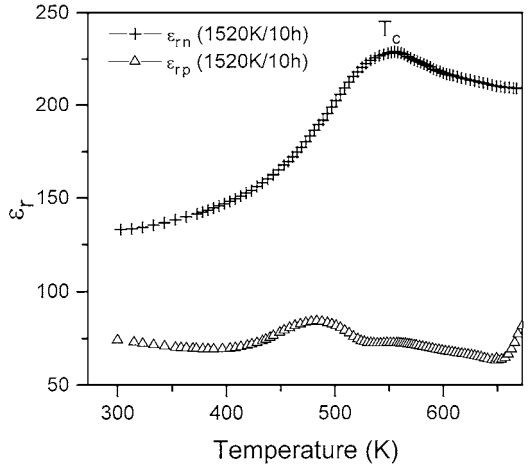

Fig. 8. The temperature dependence of ε_{rn} and ε_{rp} (at 100 kHz) for the sample 1520 K/10 h.

reflect the microstructural features, are usually the best tool to analyze their electrical properties. In the complex impedance plot (Cole-Cole; Z' vs $-Z''$ plotted in linear scale), the first semicircle in the high frequency side suggests the grain interior, while the second semicircle reflects the grain boundary effects. In some cases a third semicircle appears at very low frequencies due to the electrode—sample interface effects. Each of these semicircles could be represented by a single RC combination. A depressed semicircle whose center lies below the real axis suggests the departure from the ideal Debye like behavior. The value of bulk resistance (R_b; contribution from the grain interior) is found by the low frequency intercept of the first semicircle on the real axis (x-axis). The semicircle passes through a maximum at a frequency f_0 (relaxation frequency) and satisfies the condition

$$2\pi f_0 R_b C_b = 1$$

where C_b is the bulk capacitance (capacitance of the grain interior).

Figure 9(a)–(d) shows the impedance plots generated for the 1370 K/10 h, 1420 K/10 h, 1470 K/10 h and 1520 K/10 h samples along the direction parallel to the pressing axis. All these plots show only one semicircle in the frequency range covered (100 Hz–40 MHz)

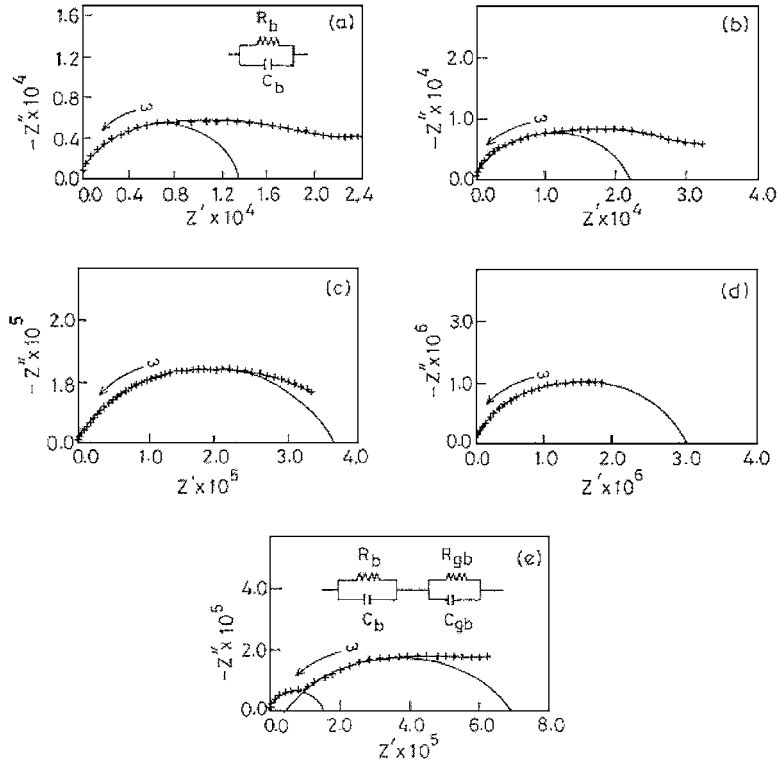

Fig. 9. Impedance plots for (a) 1370 K/10, (b) 1420 K/10 h, (c) 1470 K/10 h and (d) 1520 K/10 h samples measured along the direction parallel to the pressing axis at 670 K and (e) for the 1520 K/10 h sample measured along the direction perpendicular to the pressing axis at 670 K.

Table 2. Relaxation frequency (f_0), bulk resistance (R_b), grain boundary resistance (R_{gb}) and bulk capacitance (C_b) of the grain-oriented samples along both the directions.

Sl. no.	Sample	Measured along the direction	f_0 (Hz)	R_b (ohm)	R_{gb} (ohm)	C_b (Farad)
1	1370 K/10 h	∥ to the pressing axis	16858	1.34×10^4	–	4.90×10^{-12}
2	1420 K/10 h	∥ to the pressing axis	8030	2.23×10^4	–	8.88×10^{-10}
3	1470 K/10 h	∥ to the pressing axis	738	3.67×10^5	–	5.88×10^{-10}
4	1520 K/10 h	∥ to the pressing axis	157	3.02×10^6	–	3.36×10^{-10}
5	1520 K/10 h	⊥ to the pressing axis	63246	1.52×10^5	6.5×10^5	1.66×10^{-11}

in the present study and clearly indicate that the contribution is originating from the grain interior. The effects due to the grain boundary and the electrode are absent. This is consistent with the frequency response of the dielectric constant and dielectric loss (Fig. 6(a) and (b)). The low frequency dispersion in ε_r and D are totally absent and remains almost independent of frequency. So the electrical circuit equivalent to these samples can be regarded as a single RC combination. The values of R_b, C_b and f_0 of the grains are listed in Table 2. On the other hand the measurements made along the direction perpendicular to the pressing axis showed two semicircles corresponding to the grain interior and the grain boundary. A representative plot for the 1520 K/10 h ceramic is shown in Fig. 9(e). The microstructural characteristics (Fig. 4(a)) of these samples reveal the existence of more grain boundary regions than that obtained on the parallel direction which corroborate the impedance data. This sample can be regarded as a combination of two RC elements connected in series (shown as inset). The bulk resistance and capacitance and the grain boundary resistance (R_{gb}) of the sample in this direction are also included in Table 2. The highest relaxation frequency is normally that of grain interiors (63246 Hz), corresponding to the apex of the grain interior arc in the impedance plot, than that of the grain boundary (692 Hz). Measurements made in the perpendicular direction also showed frequency dispersion in dielectric constant and dielectric loss (Fig. 6(a) and (b)) in the frequency range in which the second semicircle appeared.

3.5. *Pyroelectric Studies*

The temperature dependency of the pyroelectric coefficient of the 1520 K/10 h sample, measured along both the parallel and perpendicular directions to the pressing axis, is shown in Fig. 10. The observed pyroelectric coefficient is negative in both the cases at

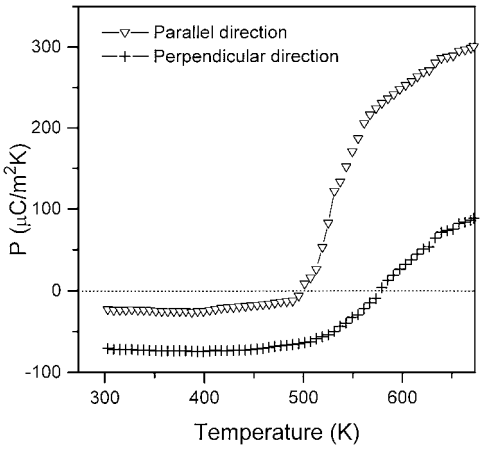

Fig. 10. Variation of pyroelectric coefficient for the 1520 K/10 h sample, with temperature measured along both parallel and perpendicular directions to the pressing axis.

300 K. There is a sudden change in the slope of the curves around the temperatures (ferroelectric to paraelectric transition temperatures) at which a maximum is observed in ε_r behavior. The sign of the pyroelectric coefficient changes from negative to positive after the transition temperature and increases on the positive side on further heating. The room temperature values of pyroelectric coefficient observed for SBT ceramics (1520 K/10 h) along the parallel and perpendicular directions to the pressing axis are -23 $\mu C/m^2K$ and -71 $\mu C/m^2K$, respectively. These values are comparable with the pyroelectric coefficients reported for the other members of the same Aurivillius family of layered oxides [47].

In ferroelectrics [48], the primary pyroelectric effect is large and expected to be negative because the spontaneous polarization decreases with increasing temperature. The secondary effect is expected to be smaller and may have either sign. The sign of the total pyroelectric coefficient depends on the dominance of any one of the (primary or secondary) pyroelectric effects. The

negative values of the total pyroelectric coefficient of the present samples at 300 K clearly indicate the dominance of primary pyroelectricity, which is akin to that of the other ferroelectric compounds [48]. The positive sign of the coefficients after the transition temperature is generally suggestive of the dominance of secondary pyroelectric effect. However, the rise in the pyroelectric coefficient is too strong to be totally suspected to be secondary effect. It may also due to a sudden release of stored charges associated with the platy microstructure. The secondary pyroelectricity originates from the contribution caused by piezoelectric (d), elastic stiffness (c) and thermal expansion (α) effects. Thus, it is possible to evaluate the primary and secondary pyroelectric coefficients separately from the known values of the constants d, c and α. Unfortunately, at this moment the availability of these data on the present system in the literature is scanty. Therefore, we have been making attempts to generate this data in order to evaluate the true pyroelectric coefficient of the present ceramic.

3.6. Ferroelectric Properties

The P vs E hysteresis loops for the partially grain-oriented ceramic (1520 K/10 h), recorded with the switching field applied in the directions parallel and perpendicular to the pressing axis are shown in Fig. 11(a)–(d). These are the loops obtained along the parallel direction recorded at 300 K and 470 K, respectively and Figs. 11(c) and (d) are in the perpendicular direction recorded at 300 K and 470 K. The value of P_r (2.96 μC/cm^2, at 300 K) is higher along the perpendicular direction than the parallel direction ($P_r = 0.214$ μC/cm^2, at 300 K), confirming that the polar axis lies in the c-plane (a or b axis). On the other hand, the coercive field is higher (2.9 kV/cm) along

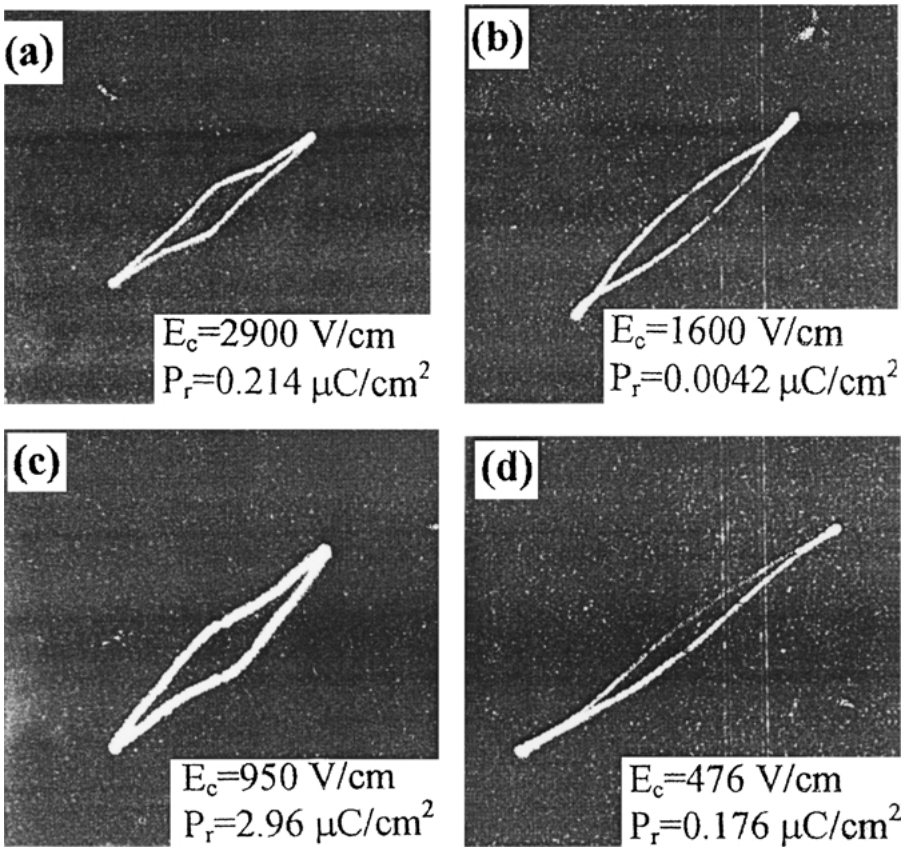

Fig. 11. The P vs E hysteresis loops for the 1520 K/10 h sample, recorded with the switching field applied in the direction parallel (a) and (b) and perpendicular (c) and (d) to the pressing axis at 300 K and 470 K.

the parallel direction, indicating that a large field is required to switch the spontaneous polarization along the c axis. The P_r and E_c of the sample recorded at higher temperature (470 K) are lower than the one recorded at 300 K along both parallel and perpendicular directions.

4. Conclusions

Grain-oriented (up to 48%) ceramics of strontium bismuth tantalate have been fabricated via cold-pressing followed by conventional sintering techniques. The orientation factor calculated from XRD studies varies with change in sintering temperature. The excessive directional grain growth in these samples at higher sintering temperatures is associated with more porosity as confirmed by SEM studies. Significant anisotropy in the dielectric constant is noticed in these partially grain-oriented ceramics. The dielectric constant measured along the direction perpendicular to the pressing axis ($\varepsilon_{rn} = 135$) is higher than that in the parallel direction ($\varepsilon_{rp} = 61$) at 100 kHz for the sample having grain-orientation factor $f = 0.44$. The dielectric constant predicted by Wiener's formula (cylindrical pores in SBT) coincides well with the experimental value for the present ceramic. The contributions from the grain interiors and the grain boundary to the observed electrical properties was studied by impedance spectroscopy and the relaxation frequency (63246 Hz) calculated for grain interiors is higher than the one calculated for grain boundary (692 Hz) for the 1520 K/10 h sample. The temperature dependence of pyroelectric coefficient was measured and studies are in progress to separate out the primary and secondary pyroelectricity in various samples along both parallel and perpendicular directions. The remnant polarization ($P_r = 2.96\ \mu C/cm^2$) of 1520 K/10 h sample measured along the perpendicular direction to the pressing axis is higher than the P_r ($0.214\ \mu C/cm^2$) measured along the parallel direction at 300 K.

Acknowledgments

The authors thank the Council of Scientific and Industrial Research (CSIR), Government of India for financial grant. We also acknowledge Mr. Vynatheya for his help in carrying out scanning electron microscopy.

References

1. J.F. Scott and C.A. Paz de Araujo, *Science*, **246**, 1400 (1989).
2. G.H. Haertling, *J. Vac. Sci. Technol.*, **9**, 414 (1990).
3. J.J. Lee, C.L. Thio, and S.B. Desu, *J. Appl. Phys.*, **78**, 5073 (1995).
4. S. Dey and R. Zuleeg, *Ferroelectrics*, **108**, 37 (1990).
5. H.N. Al-shareef, A.I. Kingon, X. Chen, K.R. Bellur, and O. Auciello, *J. Mater. Res.*, **9**, 2986 (1994).
6. W.L. Warren, D. Dimos, B.A. Tuttle, R.D. Nasby, and G.E. Pike, *Appl. Phys. Lett.*, **65**, 1018 (1994).
7. J.F. Chang and S.B. Desu, *J. Mater. Res*., **9**, 955 (1994).
8. K. Amanuma, T. Hase, and Y. Miyasaka, *Jpn. J. Appl. Phys.*, **33**, 5211 (1994).
9. P.C. Joshi and S.B. Krupanidhi, *J. Appl. Phys.*, **72**, 5827 (1992).
10. B. Aurivillius, *Ark. Kemi*, **1**, 463 (1949).
11. G.A. Smolenskii, V.A. Isupov, and A.I. Agranovskya, *Sov. Phys. Solid State*, **3**, 651 (1961).
12. E.C. Subbarao, *J. Phys. Chem. Solids*, **23**, 665 (1962).
13. C.A. Paz de Araujo, J.D. Cuchlaro, M.C. Scott, L.D. Mcmillan, and J.F. Scott, *Nature*, **374**, 627 (1995).
14. S.B. Desu and T.K. Li, *Mater. Sci. Engg*. B, **34**, L4 (1995).
15. S.B. Desu and D.P. Vijay, *Mater. Sci. Engg*. B, **32**, 75 (1995).
16. R. Dat, J.K. Lee, O. Auciello, and A.I. Kingon, *Appl. Phys. Lett.*, **67**, 572 (1995).
17. T. Li, Y. Zhu, S.B. Desu, C.H. Peng, and M. Nagata, *Appl. Phys. Lett*, **68**, 616 (1995).
18. T.C. Chen, C.L. Thio, and S.B. Desu, *J. Mater. Res.*, **12**, 2628 (1997) and references therein.
19. J.S. Yang and X.M. Chen, *Mater. Lett.*, **29**, 73 (1996).
20. S.E. Cummins and L.E. Cross, *Appl. Phys. Lett*., **10**, 14 (1967); *J. Appl. Phys*., **39**, 2268 (1968).
21. T. Takenaka, K. Shoji, H. Takai, and K. Sakata, in *Proc. Jap. Cong. Materials Research*, Tokyo (1975), p. 230, (1976), p. 212.
22. K. Sakata, T. Takenaka, and K. Shoji, *Ferroelectrics*, **22**, 825 (1978).
23. T. Takenaka and K. Sakata, in *Proc. First Meeting on Ferroelectric Materials and Their Applications*, Kyoto (1977), p. 309.
24. T. Kimura, M.H. Holmes, and R.E. Newnham, *J. Am. Ceram. Soc.*, **65**, 223 (1982).
25. M. Granahan, M. Holmes, W.A. Schulze, and R.E. Newnham, *J. Am. Ceram. Soc.*, **64**, C68 (1981).
26. A. Halliyal, A.S. Bhalla, and R.E. Newnham, *Mater. Res. Bull.*, **18**, 1007 (1983).
27. A. Halliyal, A.S. Bhalla, R.E. Newnham, and L.E. Cross, *Ferroelectrics*, **38**, 781 (1981).
28. A. Halliyal, A. Safari, A.S. Bhalla, R.E. Newnham, and L.E. Cross, *J. Am. Ceram. Soc.*, **67**, 331 (1984).
29. G. Senthil Murugan, K.B.R. Varma, Y. Takahashi, and T. Komatsu, *Appl. Phys. Lett.*, **78**, 4019 (2001).
30. F.K. Lotgering, *J. Inorg. Nucl. Chem.*, **9**, 113 (1959).
31. A. David Rae, J.G. Thompson, and R.L. Withers, *Acta Cryst.* B, **48**, 418 (1992).
32. C.B. Sawyer and C.H. Tower, *Phys. Rev.*, **35**, 269 (1930).
33. R.L. Byer and C.B. Roundy, *Ferroelectrics*, **3**, 333 (1972).
34. V.N. Sigaev, E.V. Lopatina, P.D. Sarkisov, S. Yu. Stefanovich, and V.I. Molev, *Mater. Sci. Engg.* B, **48**, 254 (1997).
35. K. Shantha and K.B.R. Varma, *Mater. Res. Bull*., **32**, 1581 (1997).
36. C.H. Lu and B.K. Fang, *J. Mater. Res*., **13**, 2262 (1998).

37. W. Buessem, L.E. Cross, and A.K. Goswami, *J. Am. Ceram. Soc.*, **49**, 34 (1966).
38. G. Haertling, *Am. Ceram. Soc. Bull.*, **45**, 1084 (1966).
39. K. Shoji, M. Aikawa, Y. Uehara, and K. Sakata, *Jpn. J. Appl. Phys.*, **37**, 5273 (1998).
40. H. Frolich, *Theory of Dielectrics* (Clarendon Press, Oxford, 1949).
41. K. Lichtenecker, *Phys. Zeitsch*., **27**, 115 (1926).
42. N. Wiener, *Phys. Zeitsch*., **5**, 332 (1904).
43. N. Wiener, *Leipzig Ber*., **61**, 113 (1909).
44. F.A. Diaz and L.E. Cross, *Ferroelectrics*, **17**, 405 (1977).
45. F. Micheron, *Revue Technique Thomson-CSF*, **4**, 5 (1972).
46. J.F. Berton and B. Roelandt, *Bull. Soc. Fr. Ceram*., **94**, 51 (1972).
47. T. Takenaka and K. Sakata, *Ferroelectrics*, **118**, 123 (1991).
48. A.S. Bhalla and R.E. Newnham, *Phys. Stat. Sol.* (a), **58**, K19 (1980).